Crystal structure of *Mycobacterium tuberculosis* SecA, a preprotein translocating ATPase

Vivek Sharma*†‡, Arulandu Arockiasamy†‡, Donald R. Ronning†§, Christos G. Savva¶, Andreas Holzenburg†¶, Miriam Braunstein‖, William R. Jacobs, Jr., and James C. Sacchettini*†,††**

*Center for Structural Biology, Institute of Biosciences and Technology, Houston, TX 77030; †Department of Biochemistry and Biophysics, Texas A&M University, College Station, TX 77843-2128; ¶Microscopy and Imaging Center and Department of Biology, Texas A&M University, Biological Sciences Building West, College Station, TX 77843-2257; ‖Department of Microbiology and Immunology, University of North Carolina, Chapel Hill, NC 27599; and **Howard Hughes Medical Institute, Department of Microbiology and Immunology, Albert Einstein College of Medicine, 1300 Morris Park Avenue, Bronx, NY 10461

Communicated by William T. Wickner, Dartmouth Medical School, Hanover, NH, December 12, 2002 (received for review November 18, 2002)

In bacteria, the majority of exported proteins are translocated by the Sec system, which recognizes the signal sequence of a preprotein and uses ATP and the proton motive force to mediate protein translocation across the cytoplasmic membrane. SecA is an essential protein component of this system, containing the molecular motor that facilitates translocation. Here we report the three-dimensional structure of the SecA protein of *Mycobacterium tuberculosis*. Each subunit of the homodimer contains a ''motor'' domain and a translocation domain. The structure predicts that SecA can interact with the SecYEG pore and function as a molecular ratchet that uses ATP hydrolysis for physical movement of the preprotein. Knowledge of this structure provides a framework for further elucidation of the translocation process.

Protein translocation across cell membranes is a facilitated process performed by a multiprotein translocase with ATP binding and hydrolysis as the driving force for transport (1, 2). The translocase is part of an evolutionarily conserved system of protein translocation across membranes found in all bacteria, eukaryotes, and archaea (3, 4). Through genetic and biochemical studies, an understanding of the mechanism of the Sec translocation is emerging (5–7). Proteins destined for transport across the cytoplasmic membrane are synthesized as precursors, called preproteins, distinguished by the presence of an amino-terminal signal. In bacteria, the Sec translocon represents the minimal essential component necessary for export and is comprised of the transmembrane protein conduction pore SecYEG and the peripheral membrane ATPase (8, 9).

SecA is a multifunctional protein that plays a central role in the export pathway. The protein interacts with acidic phospholipids in the membrane, the SecYEG pore, and chaperones, such as SecB, that deliver preproteins to the translocase (10–12). The binding of preproteins by SecA is an early step in protein export (13). SecA is generally thought to undergo a conformational change on binding of ATP, which has been proposed to promote insertion of SecA and the bound precursor into the membrane translocase pore (5, 14, 15). One proposal for the subsequent events suggests that on ATP hydrolysis SecA deinserts and releases the translocating substrate, which remains associated with the core translocase. Through multiple rounds of ATP binding and hydrolysis, SecA moves between the ''inserted'' and ''deinserted'' state, resulting in processive translocation along the precursor substrate and export of the translocating protein across the membrane in 20- to 30-aa increments (14, 16). The deinsertion of SecA is facilitated by the proton motive force (17) that can complete the process even in the absence of SecA and ATP (14). Auxiliary proteins that aid in translocation include SecD, SecF, YajC, and YidC (18).

Sequence alignments have revealed a conserved ATPase domain in the amino-terminal half of SecA (residues 2–221 and 360–587). This domain shares significant structural similarity with the DEAD motor domains of helicases and, by analogy, characteristics common to the more distant motor domains of kinesins and myosin (19). Molecular motors such as these generate force that is translated into movement by the binding of ATP and/or release of ADP and phosphate. The power stroke in these molecular motors is provided by the movement (usually a rotation) of two juxtaposed nucleotide interacting regions of the protein, induced by specific interactions to ATP, the so-called ''switch-on'' phase. By virtue of the loss of key noncovalent interactions between the protein and γ-phosphate of ATP, ATP hydrolysis has been shown to induce conformational changes in the reverse direction, realigning the two nucleotide binding regions in the so-called ''switch-off'' phase of the motor. This movement is typically linked to other structural components of the protein that magnify the extent and change the direction of the motor movements. Indeed, protein structural elements attached to the motor domains have been described as connectors, levers, and amplifiers, to explain how the relatively simple movements of the two nucleotide binding regions transmit their force and movement to generate large alterations in structure (19).

The motor domains of SecA, the SecYEG pore proteins, and the signal sequences of nascent peptides are all highly conserved in bacteria; however, other elements of SecA-dependent translocation may be less well conserved. Some Gram-positive bacteria as well as *Mycobacterium* species contain two homologous SecAs with nonoverlapping functions (20). In *Mycobacterium tuberculosis*, the essential SecA1 is the homolog believed to be equivalent to the *Escherichia coli* SecA (throughout this manuscript we will refer to mycobacterial SecA1 as *tb*SecA). In contrast, SecA2 from both *Listeria monocytogenes* (21) and *M. tuberculosis* (20) are not essential, but are required for full virulence (M.B. and W.R.J., unpublished results). In *Streptococcus gordonii* (22), *L. monocytogenes*, and *Mycobacterium smegmatis*, some of the proteins exported by SecA2 possess classical tripartite N-terminal signal sequences, but it is not known how these signals are distinguished from those exclusively recognized by SecA. Another paradox of the SecA2-dependent pathway in *M. tuberculosis* is the fact that at least two of the secreted proteins lack signal sequences (M.B., unpublished results). In this study, we report the structure of the *tb*SecA in the free form and with bound ADP-β-S. Comparison of the structure with the recently

Abbreviations: *bs*SecA, *Bacillus subtilis* SecA; EM, electron microscopy; HCD, helical core domain; NBD, nucleotide binding domain; SSD, substrate specificity domain; *tb*SecA, mycobacterial SecA1.

Data deposition: The atomic coordinates of SecA and SecA:ADP-β-S have been deposited in the Protein Data Bank, www.rcsb.org (PDB ID codes 1NL3 and 1NKT).

‡V.S. and A.A. contributed equally to this work.

§Present address: Laboratory of Molecular Biology, National Institute of Diabetes and Digestive and Kidney Diseases, National Institutes of Health, Bethesda, MD 20892.

††To whom correspondence should be addressed at: Department of Biochemistry and Biophysics, Texas A&M University, 2128 TAMU, College Station, TX 77843-2128. E-mail: sacchett@tamu.edu.

Table 1. Data and refinement statistics

Data statistics						Refinement statistics		
Dataset	Wavelength, Å	Resolution range, Å*	Unique reflections*	Completeness, %*	R_{merge}*		APO	ADP-β-S
Se-1	0.9611	100.0–3.0 (3.11–3.0)	64,805 (3,801)	91.7 (53.9)	0.092 (0.31)	Protein nonhydrogen atoms	13,283	13,264
Se-2	0.9797	100.0–3.0 (3.11–3.0)	52,794 (1,563)	74.5 (22.0)	0.079 (0.29)	Solvent molecules	930	752
Se-3	0.9800	100.0–3.0 (3.11–3.0)	55,356 (1,913)	78.3 (27.1)	0.080 (0.28)	Resolution range, Å	8.0–2.8	99–2.6
Se-4	1.00348	100.0–3.0 (3.11–3.0)	63,318 (3,349)	89.9 (47.6)	0.091 (0.32)	Total reflections ($F > 1\sigma F$)	82,072	105,541
ADP-β-S	1.0332	100.0–2.4 (2.49–2.40)	139,810 (13,803)	98.1 (98.2)	0.089 (0.48)	Total reflections (R_{free})	4,386	5,631
						R_{cryst}	0.192	0.213
						R_{free}	0.259	0.265
APO	1.0332	100.0–2.75 (2.85–2.75)	95,337 (8,700)	98.8 (91.9)	0.096 (0.461)	rmsd of bond lengths, Å	0.01	0.02
						rmsd of bond angles, °	1.43	1.56
						Average protein B-factor, Å^2	46.13	16.12

*Values in the highest-resolution shell are included in parentheses.

reported structure of *Bacillus subtilis* SecA (*bs*SecA) (23) provides insights into the mechanism of translocation.

Methods

Cloning and Purification. *secA1* was amplified by PCR from *M. tuberculosis* H37Rv genomic DNA and cloned into the T7 expression plasmid pET29a (Novagen). This expression construct encodes a *tb*SecA protein lacking the most C-terminal 57 aa and containing 31 vector derived amino acids fused at the N terminus. Protein was expressed in *E. coli* at 16°C by using standard conditions. The cell lysate supernatant was applied to a Blue Sepharose column and eluted with a NaCl gradient. A 60% ammonium sulfate precipitation followed by chromatography on Q Sepharose resin was used to produce protein of high purity. A Superdex S-200 gel-filtration column (Amersham Pharmacia) was used to remove any remaining contaminants.

Crystallization and Data Collection. Diffraction-quality crystals of *tb*SecA were obtained from solution of 10 mM Tris·HCl (pH 7.5), 3.5–3.7 M sodium formate, and 5–10% glycerol, in the hanging drop method (see *Expression, Purification, and Crystallization* in *Supporting Text*, which is published as supporting information on the PNAS web site, www.pnas.org). In the case of cocrystallization with the nucleotide analog (ADP-β-S), protein was preincubated with 1–2 mM of nucleotide, and 2–4 mM of $MgCl_2$. *tb*SecA crystallized in the hexagonal space $P6_222$ with cell parameters $a = 205.9$ Å, $b = 205.9$ Å, and $c = 292.8$ Å, and two molecules of *tb*SecA in the asymmetric unit. Data sets were collected at synchrotron beam lines BioCARS 14-BM-C and -D, 14-ID-B, and SBC 19-ID-D of the Advanced Photon Source (Argonne National Laboratory, Chicago) and the Advanced Light Source (Berkeley Lab, Berkeley, CA) and processed by using DENZO and SCALEPACK (24).

Structure Determination. Multiwavelength anomalous dispersion (MAD) phasing (25) was used with diffraction data collected from a selenomethionylated *tb*SecA crystal at four different wavelengths such that dispersive and Bijvoet differences due to Se atoms were maximized (Table 1). A combination of computational methods, including SOLVE (26), SHARP (27), and CCP4 (28), was used to locate and subsequently refine 46 of 50 Se sites. Solvent flattening improved the electron density map, and an initial protein model was constructed using O (29) and refined to an R_{cryst} of 0.34 and an R_{free} of 0.39 against MAD data at 3.25 Å by using CNS (30). These coordinates were then refined against native *tb*SecA diffraction data and manually adjusted by using subsequent $2F_{obs} - F_{calc}$ electron density maps and unbiased electron density maps (31). Final models were produced through several cycles of manual model building and refinement in REFMAC5, a part of CCP4 (ref. 28; Table 1).

Results and Discussion

Structure Determination. The apo-structure of *tb*SecA was built into electron density maps calculated to 2.8 Å by using MAD data from crystals of selenomethionylated proteins. Diffraction data on a *tb*SecA:Mg^{2+}:ADP-bound complex were collected to 2.6 Å from crystals that were nearly isomorphous to apo-*tb*SecA (Table 1). In all cases the recombinant *tb*SecA protein used for crystallization and electron microscopy (EM) studies contained an N-terminal extension of 31 residues from the expression vector and lacked 57 residues at the C terminus. There are two molecules of *tb*SecA in the asymmetric unit. The first 14 residues of the N-terminal vector-derived extension, as well as residues 720–729 and 836–892 of *tb*SecA were not visible in electron density maps of either molecule. Thus, the final coordinates for both protein structures reported here contain 17 residues from the N-terminal extension and 825 (of 949) residues of mature *tb*SecA.

Overall Structure of a *tb*SecA Subunit. The structure of *tb*SecA consists of 30 α-helices and 20 β-strands organized into two globular structural domains (Fig. 1). The motor domain of *tb*SecA is composed of residues 2–221 and 360–587, and the translocation domain consists of residues 222–359 and 587–835. Two α/β-sheets make the motor domain, which is similar in structure to the DEAD motor ATPases reported for other proteins involved in structural movements related to their function. These α/β-sheets have been referred to in the literature as *n*ucleotide *b*inding *d*omains NBD1 and NBD2, the latter having also been referred to as IRA2 (32, 33). NBD1 consists of a seven-stranded β-sheet (β1–5, β13–14) surrounded by 12 α-helices (α1–10, α15–16). NBD2 is composed of a six-stranded β-sheet (β15–20) and six surrounding α-helices (α17–22). The closest structural homolog in the protein databank for NBD1 is the motor domain of the yeast initiation factor (PDB ID code 1QVA) and for NBD2, it is RecG helicase (PDB 1GM5). When the entire motor domain is used to search the available protein database, the most similar polypeptide folds are found for the family of RNA and DNA helicases, including HCV RNA helicase (PDB 1HEI), and the DNA helicases (PDB 1PJR), and a RecG helicase (PDB 1GM5).

No structural homologs were found for the translocation domain in a VAST structural homology search (www.ncbi.nlm.nih.gov/Structure/VAST/vastsearch.html). Using accepted nomenclature, the translocation domain is composed of the *s*ubstrate *s*pecificity *d*omain [SSD (33); or, as it is commonly referred to, preprotein binding domain] and the *h*elical *c*ore *d*omain

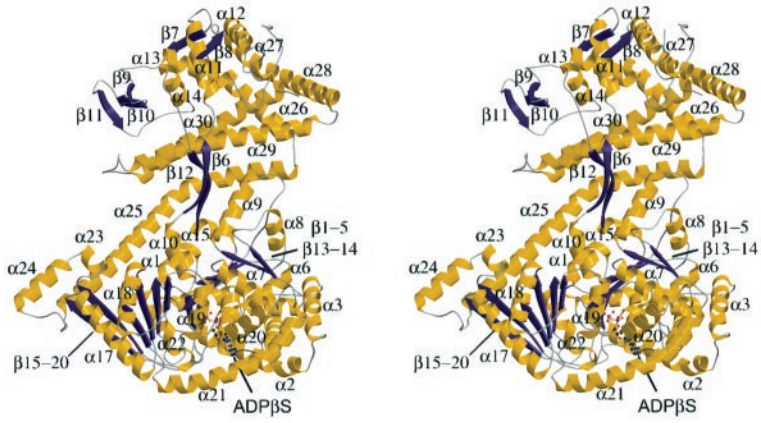

Fig. 1. The crystal structure of SecA ATPase from *M. tuberculosis*. The stereo ribbon representation of the ADPβS-bound protomer is colored based on the secondary structure.

(HCD, also referred to as IRA1). The SSD has been shown to bind the signal sequence of the preprotein and is made up of residues 222–359, inserted in NBD1 (33, 34). The globular part of SSD packs next to the C-terminal HCD and it is composed of four α-helices (α11–α14) and five β-strands (β7–β11). The translocation domain is highly porous with some 100 water molecules found buried in the structure. Two long antiparallel β-strands, β6 and β12, connect the globular part of SSD from the translocation domain to helices α10 and α15 of NBD1. The longest helix, α25 ($\approx$50 residues), connects NBD2 to the HCD region.

The two molecules of *tb*SecA contained within a single asymmetric unit are virtually identical [rms deviation (rmsd) for Cα = 1.35 Å]. This is also true when you compare the overall backbone trace of apo-*tb*SecA with the structure of the protein with bound ADP-β-S, suggesting that the ADP binding does not significantly change the structure. The only minor backbone differences were observed in the regions of the C-terminal core helices. Electron density maps calculated with data from crystals of the *tb*SecA:ADP-β-S:Mg^{2+} complex show clear electron density for a single molecule of the ADP analog, and the Mg^{2+} bound at the interface between NBD1 and NBD2 of the motor domain. Three side chains (Q80, D493, and D501) that interact with ADP-β-S show significant conformational differences between the apo and ADP-β-S-bound forms of the proteins.

Superimposition of our structure with *bs*SecA (802 residues) structure shows it shares a similar fold (rmsd of 2.47 Å for 720 Cα atoms). [See *Superimposition of Mycobacterial SecA1* (tb*SecA*) with Bacillus subtilis *SecA* (bs*SecA*) in *Supporting Text* and Fig. 6, which is published as supporting information on the PNAS web site.] The smaller size of *bs*SecA is primarily due to the absence of α20 and α21, which are not found in the SecA sequences of Gram-negative bacteria. The structure of *tb*SecA was clearly visible for the 148 residues marked as unreliable in the *bs*SecA structure. Overall, the translocation domains of the two structures superimpose less well than the motor domains with significant (>2 Å) shifts for residues in SSD.

***tb*SecA Dimer.** Examination of the crystal packing, as well as 3D EM reconstructions of *tb*SecA taken under conditions similar to those used in crystallization, shows that *tb*SecA forms a tetramer of approximate D2 symmetry (Fig. 2). In the crystal structure, the molecules that form the A–B dimer (Fig. 3 *b* and *e*) bury 1,290 $Å^2$ of the accessible surface area of each subunit (3.2%), and the residues involved in forming these contacts are highly conserved (E^{313}, R^{323}, L^{602}, L^{604}, L^{608}, I^{614}, E^{615}, M^{618}, R^{621}, E^{791}, G^{792}, L^{795}, and M^{798}) and primarily hydrophobic in agreement with a recent finding that dimers of SecA can be dissociated in the presence of detergents or lipids (35). The A–C dimer (Fig. 3 *c* and *f*) buries $\approx$1,845 $Å^2$ of each subunit (4.5%). These interactions are mostly polar in nature and are from regions that are not well conserved in SecA sequences and, in fact, include some of 17 residues from the recombinant expression vector. Subtraction of the surface area buried by these 17 residues leaves only 730 $Å^2$ of the A–C dimer interface buried (1.8%).

For *bs*SecA (see Fig. 3 *a* and *c*), the two subunits of the dimer are arranged in a configuration somewhat intermediate to the

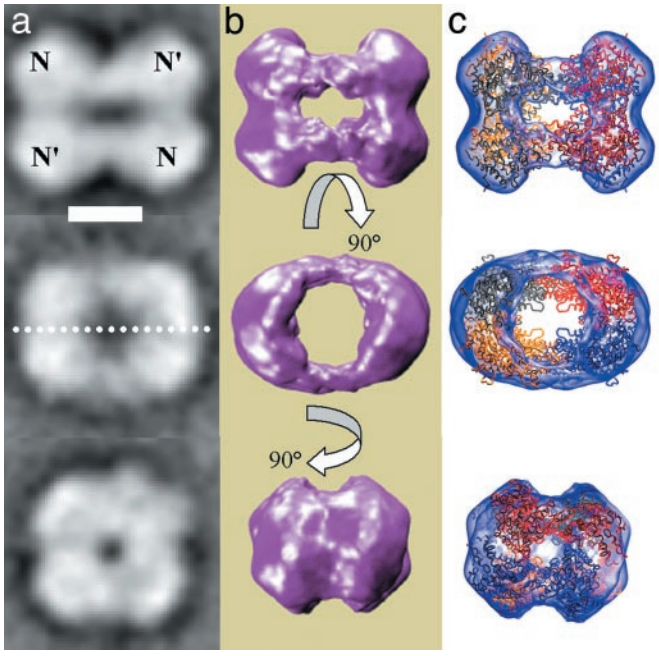

Fig. 2. Single-particle reconstruction of *tb*SecA and docking with crystal structure. (*a*) Average projections of *tb*SecA. (*b*) Surface rendering of EM 3D reconstruction. (*c*) Docking of EM 3D map with crystal structure. Rows from top to bottom represent the three most significant projections observed: side view 1, side view 2, and end-on view. For ease of orientation densities contributing to the motor domains are highlighted (N dimer above and N′ dimer below the plane) with the dimer–dimer interface residing within the plane of the paper. With side view 2, the dimer–dimer interface is highlighted by a dashed line. (Scale bar, 50 Å.) For additional details, see *Single-Particle Electron Microscopy* in *Supporting Text* and Fig. 7, which is published as supporting information on the PNAS web site.

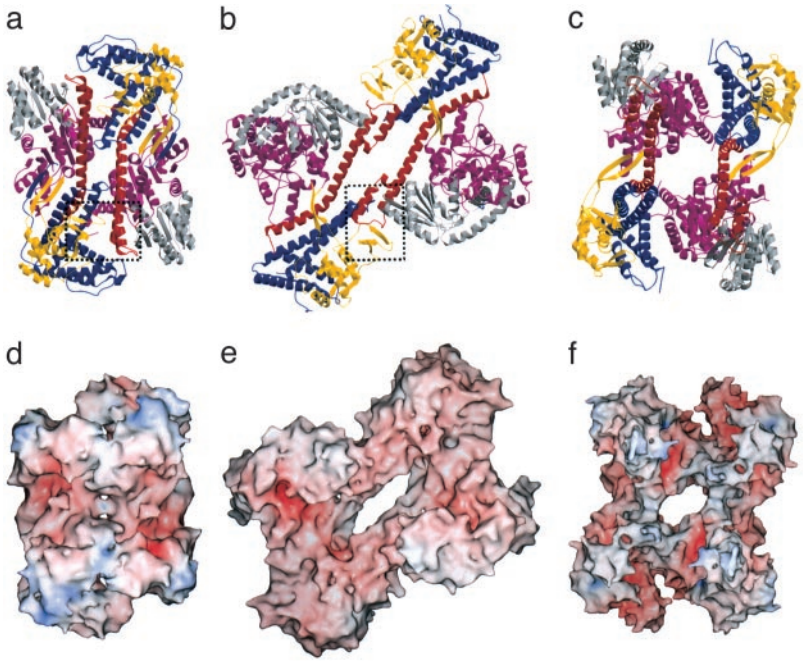

Fig. 3. Dimer formation of SecA ATPase. The ribbon representations of *bs*SecA (*a*) and the A–B (*b*) and A–C (*c*) dimers of *tb*SecA are colored according to the functional regions of the protein. The ATPase motor domain consists of NBD1 (purple) and NBD2 (gray). The translocation domain consists of the preprotein binding SSD domain (yellow) and helical HCD domain (blue). The long α25-helix and short segments associated with the pump mechanism are shown in red. (*d–f*) The molecular surface of the corresponding SecA dimers colored according to the electrostatic potential on the surface in orientations identical to that in *a*, *b*, and *c*, respectively. The proposed mycobacterial A–B dimer (*b* and *e*) contains an elliptical pore, which we believe aligns with the integral membrane channel of SecYEG. Also visible is the bound molecule of ADP-β-S as a ball-and-stick model. The dimer interfaces of *bs*SecA (*a*) and *tb*SecA (*b*) are marked by a box, and a more detailed view is provided in Fig. 8, which is published as supporting information on the PNAS web site.

A–B and A–C dimers observed for *tb*SecA (Fig. 3). However, the interface of the *bs*SecA dimer is very similar to that of the A–B dimer (Fig. 3 *a* and *b*). Specifically the helices α24 and α25 of one subunit forms contacts with the loops at the end of a small β-sheet (β9–β11) of the translocation domain. However, the interface for *bs*SecA is on the opposite side of the β-sheet as the interface of the *tb*SecA. This suggests that the A–B dimer is most similar to the active form of *tb*SecA.

Although we cannot rule out the possibility that SecA functions as a monomer or even a tetramer, as suggested by previous studies (35, 36), the structure of the A–B dimer suggests that this is the active form. The two subunits of the A–B dimer are related by a nearly perfect twofold axis of symmetry perpendicular to a plane defined by an elliptical pore found in the center of the dimer (Fig. 3). The size of the pore (10×35 Å) is similar to that observed in a recent EM structure of the SecYEG complex from *E. coli* (16×25 Å) (9). Examination of the dimer from the side-view shows that one face of the dimer is relatively convex and the other is slightly concave. On the convex side, protein chains extend $\approx$25 Å above the plane of the pore. The ATP/ADP binding sites are solvent exposed on the outer rim of the dimer. Examination of both surfaces of the dimer suggests that SecA docks on SecYEG via its concave surface. This orientation would put the majority of the translocation domain, except for the putative preprotein binding region, in contact with SecYEG, consistent with previous results (37, 38).

ATPase Active Site and Proposed Mechanism. At a molecular level the concerted movements associated with ATP coupled motors usually result from relatively small rigid-body movements of structural elements coupled to either the ATP or ADP bound states. In fact, most of the changes in the relative orientation of the nucleotide binding motifs are linked to a few key interactions that occur with residues of the NBDs and the γ-phosphate of ATP. For example, in myosin the movements of the motor domain are coupled to long α-helical "levers" that alter the direction and magnify the extent of the motor domain changes. DNA and RNA helicases also possess molecular motors with similar components, although the motion of the domains are not directly linked to α-helical levers.

The molecular motors of SecA are structurally most similar to the DEAD motor domains of the DNA/RNA helicase family of proteins (39–41). When NBD1 of *tb*SecA with bound ADP-β-S-Mg^{2+} is superimposed with the comparable region of the PcrA DNA helicase with bound ATP-Mg^{2+} and PcrA helicase with bound SO_4, representing the "switch-on" and "switch-off" states of these helicase motor domains, respectively, the motor domain of *tb*SecA with ADP-β-S-Mg^{2+} most closely aligns to the PcrA-SO_4 structure. This is also true for the structure of the apo-*tb*SecA. Studies defining the conformational changes in the motor domains of PcrA indicate that the motor undergoes a rotation of $\approx$10° in the relative orientation of two NBDs going from the ATP-bound to the SO_4-bound form, which is thought to represent the motor transition from the ATP- to the ADP-bound forms of PcrA (42). This rotation seems to result solely from a set of new binding interactions between the γ-phosphate of ATP and Gln-254, Arg-287, and Arg-610 of PcrA's NBD2. A comparison of the structures of PcrA and *tb*SecA:ADP-β-S:Mg^{2+} shows that the amino acid residues that interact with the γ-phosphate of ATP are conserved in *tb*SecA (Fig. 4). In the ADP-β-S-bound *tb*SecA structure, the side chains of these conserved residues are too far away from the modeled position of the γ-phosphate to bond, in fact they are in a position similar to what is observed in the PcrA-SO_4. A rotation of a similar magnitude and direction to that observed for the PcrA-SO_4 and PcrA-ATP transition would move in *tb*SecA the side chains of R490, R570, and Q566 in hydrogen bonding distance to the γ-phosphate of a modeled ATP.

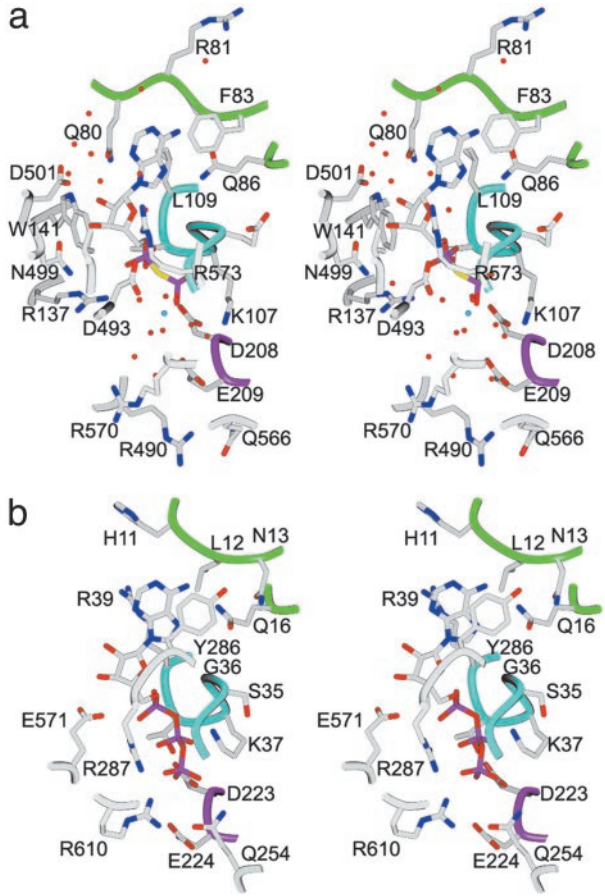

Fig. 4. Comparison of the binding site of *tb*SecA:ADP-β-S (*a*) with PcrA:ATP (*b*). (*a*) Stereo diagram of a stick representation of the binding site of *tb*SecA:ADP-β-S shows the residues involved in the ADP binding. Most of the contacts from NBD1 are from Walker A (cyan), Walker B (purple), and adenine binding (green) loops. (*b*) Similar representation of binding of ATP analog ADPNP to PcrA helicase (42). The side chains that make contact with the γ-phosphate are Q254, R287, and R610 and have counterparts in SecA (Q566, R490, and R570).

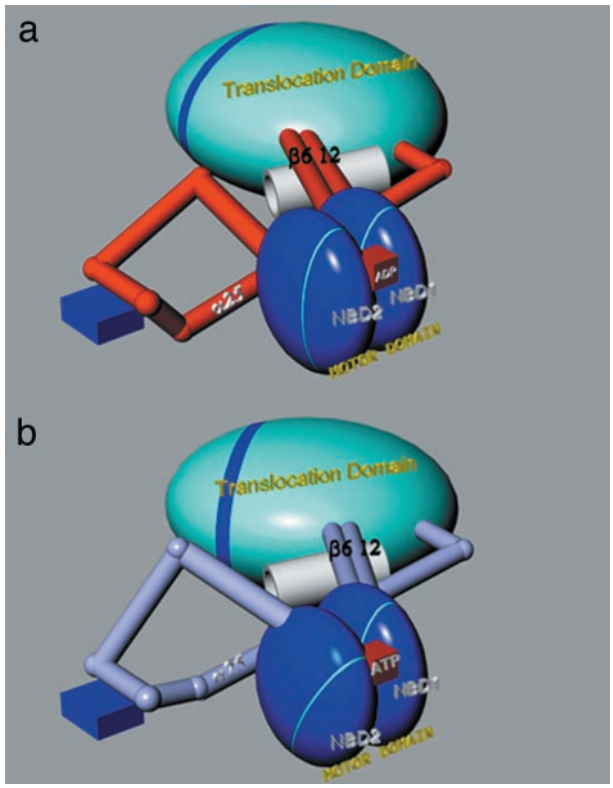

Fig. 5. A mechanical drawing depicting our model of the motor movements associated with the ADP and ATP bound states of SecA. (*a*) The red tubes represent the regions of the connecting structure of SecA observed in the ADP bound state. (*b*) In transparent violet are the corresponding regions of our model of the protein with ATP bound. The movements of the motor domain as described in the text are transmitted to the translation domain via the long α25-helix and the two connecting β-strands shown atop the silver pipe, which is the conserved pore found in the SSD. In dark blue is the pivot arm groove from the adjacent subunit of the dimer.

The relatively small predicted rotation between NBD1 and NBD2 for the DEAD motor of SecA is likely to be transformed into a much larger movement of the relative positions of the motor and translocation domains and results in alterations to the SecA pore and preprotein binding region. NBD2 of the motor domain is connected by an extension of a core β-strand β20, and a series of short segments of coil and α-helices, to a 50-residue-long α-helix (α25) that serves as a linkage between the motor domain to the translocation domain. α25-helix contributes most of the residues that line the elliptical pore in the center of the dimer. Together, the short α-helices and coil segments, along with α25, resemble a mechanical hand pump. In such a mechanical device, the short α-helix, α24, would represent the pump handle and the subsequent 90° opposed coil would be a pivot arm; in fact, it lies in a groove on the translocation domain of the other subunit of the dimer. The short coil that connects the pivot arm to α25 is at an angle of 70° relative to the α25-helix. This assembly would be equivalent to what in simple motor terminology is described as an inclined plane, where the short coil is somewhat analogous to the offset provided by a cam gear relative to the piston rod, similar to the relationship of the crankshaft and the connecting rod of a piston-driven motor.

Unlike typical piston-driven motors, which rotate a full 360°, the motion of NBD2 relative to NBD1 during ATP cycling would be a simple back and forth motion. β20 of NBD2 serves as the connection of the DEAD motor to the handle of the pump and "raises and lowers" the pump handle with relative short strokes. The rotation of the pivot arm around the groove would change the direction of movement to a longitudinal translational motion, via the offset cam and the long α-helix. Without additional structural information it is impossible to know whether the net result of this rather simple machine is an up–down motion of α25, a twisting motion to the helix, or a movement along the axis of α25. However, the relatively large differences in the length of handle (α24), compared with that of the connecting rod α25-helix, and the short offset cam suggest that even small strokes of the handle could in fact provide for very large movements in α25.

Because the α25-helix is one of only three connections between the motor and translocation domains, the pump movement is likely to effect the orientation of the translocation domain relative to the motor domain. This movement may also be propagated to the two β-strands (β6 and β12) that cross over from the core of NBD1 to the preprotein (SSD) region of the translocation domain. Specifically, the two connecting β-strands transverse the α25-helix, nearly perpendicular to the axis of the helix, and there are a number of hydrogen bonding interactions between the two β-strands and the helix, suggesting that the two β-strands may be tethered to the α25-helix such that any movement of α25, as described above, could serve to move the β-strands as well as the entire SSD relative to the HCD.

There are several possible mechanisms that can be invoked to correlate structure and previous biochemical studies with protein translocation. One mechanism builds on the previously proposed ratchet mechanism for protein translocation (43) and is consistent with the proposed movement of α25 and the linkage of this movement to the β-strands of the preprotein binding region. There is ample evidence that the signal peptide binds to the SSD (33, 44). A probable binding site would be between the β-strands and the remainder of the translocation domain. In support of this notion, there is a solvent-filled channel that lies between the connecting β-strands and the rest of the translocation domain. This pore is also found in the *bs*SecA. The translation of the α25-helix in response to ATP binding could move the two connecting β-strands outward, away from the SecA pore at the center of the dimer (Fig. 5). On ATP hydrolysis the α25-helix and the two connecting β-strands would return to the position observed in the structures presented. This movement would effectively push a section of the preprotein toward the central pore of the dimer. Movement of the relative orientation of the protomers could serve to potentiate this motion. If, as we believe, the pore of the SecA dimer aligns with the integral membrane channel created by SecYEG, successive cycles of the associated movements of these regions with ATP binding and hydrolysis would permit the entire protein to be translocated through the SecYEG membrane channel. In this case we would envisage that a contraction in the SecA pore or interactions of the preprotein with SecYEG could hold the partially translocated preprotein in place ensuring one-way movement. This mechanism does not require very large conformational changes of SecA for translocation to occur, nor does it involve insertion and deinsertion of SecA, although it does not rule out either possibility. Additional biochemical data are required to further define the mechanics and thermodynamics of SecA-mediated protein translocation.

We thank Dr. Robert Droleskey of the U.S. Department of Agriculture/Agricultural Research Service/Southern Plains Agricultural Research Center for use of the Hitachi microscope, Dr. Michael Schatz of Image Science (Berlin) for help with IMAGIC software, Brett Owens for technical assistance, and Ms. Linda Fisher for preparation of the manuscript. Use of the Argonne National Laboratory Structural Biology Center beamlines at the Advanced Photon Source was supported by the U.S. Department of Energy, Office of Energy Research, under Contract W-31-109-ENG-38. Use of the BioCARS Sector 14 was supported by the National Institutes of Health, National Center for Research Resources. This work was supported by the Robert A. Welch Foundation and National Institutes of Health Grant GM62410.

1. Driessen, A. J., Manting, E. H. & van der Does, C. (2001) *Nat. Struct. Biol.* **8,** 492–498.
2. Economou, A. (2000) *FEBS Lett.* **476,** 18–21.
3. Matlack, K. E., Mothes, W. & Rapoport, T. A. (1998) *Cell* **92,** 381–390.
4. Pohlschroder, M., Prinz, W. A., Hartmann, E. & Beckwith, J. (1997) *Cell* **91,** 563–566.
5. Economou, A. & Wickner, W. (1994) *Cell* **78,** 835–843.
6. Manting, E. H. & Driessen, A. J. (2000) *Mol. Microbiol.* **37,** 226–238.
7. Mori, H. & Ito, K. (2001) *Trends Microbiol.* **9,** 494–500.
8. Brundage, L., Fimmel, C. J., Mizushima, S. & Wickner, W. (1992) *J. Biol. Chem.* **267,** 4166–4170.
9. Breyton, C., Haase, W., Rapoport, T. A., Kuhlbrandt, W. & Collinson, I. (2002) *Nature* **418,** 662–665.
10. Hartl, F. U., Lecker, S., Schiebel, E., Hendrick, J. P. & Wickner, W. (1990) *Cell* **63,** 269–279.
11. Hendrick, J. P. & Wickner, W. (1991) *J. Biol. Chem.* **266,** 24596–24600.
12. Woodbury, R. L., Topping, T. B., Diamond, D. L., Suciu, D., Kumamoto, C. A., Hardy, S. J. & Randall, L. L. (2000) *J. Biol. Chem.* **275,** 24191–24198.
13. Cunningham, K. & Wickner, W. (1989) *Proc. Natl. Acad. Sci. USA* **86,** 8630–8634.
14. Schiebel, E., Driessen, A. J., Hartl, F. U. & Wickner, W. (1991) *Cell* **64,** 927–939.
15. Economou, A., Pogliano, J. A., Beckwith, J., Oliver, D. B. & Wickner, W. (1995) *Cell* **83,** 1171–1181.
16. van der Wolk, J. P., de Wit, J. G. & Driessen, A. J. (1997) *EMBO J.* **16,** 7297–7304.
17. Nishiyama, K., Fukuda, A., Morita, K. & Tokuda, H. (1999) *EMBO J.* **18,** 1049–1058.
18. Nouwen, N. & Driessen, A. J. (2002) *Mol. Microbiol.* **44,** 1397–1405.
19. Kull, F. J., Sablin, E. P., Lau, R., Fletterick, R. J. & Vale, R. D. (1996) *Nature* **380,** 550–555.
20. Braunstein, M., Brown, A. M., Kurtz, S. & Jacobs, W. R., Jr. (2001) *J. Bacteriol.* **183,** 6979–6990.
21. Lenz, L. L. & Portnoy, D. A. (2002) *Mol. Microbiol.* **45,** 1043–1056.
22. Bensing, B. A. & Sullam, P. M. (2002) *Mol. Microbiol.* **44,** 1081–1094.
23. Hunt, J. F., Weinkauf, S., Henry, L., Fak, J. J., McNicholas, P., Oliver, D. B. & Deisenhofer, J. (2002) *Science* **297,** 2018–2026.
24. Otwinowski, Z. & Minor, W. (1997) *Methods Enzymol.* **276,** 307–326.
25. Hendrickson, W. A. (1991) *Science* **254,** 51–58.
26. Terwilliger, T. C. (1994) *Acta Crystallogr. D* **50,** 17–23.
27. de la Fortelle, E. & Bricogne, G. (1997) *Methods Enzymol.* **276,** 472–494.
28. Collaborative Computational Project Number 4 (1994) *Acta Crystallogr. D* **50,** 760–763.
29. Jones, T. A., Zhow, J. Y., Cowan, S. W. & Kjeldgaard, M. (1991) *Acta Crystallogr. A* **47,** 110–119.
30. Brunger, A. T., Adams, P. D., Clore, G. M., Delano, W. L., Gros, P., Grossekunstleve, R. W., Jiang, J. S., Kuszewski, J., Nilges, M., Pannu, N. S., *et al.* (1998) *Acta Crystallogr. D* **54,** 905–921.
31. Kantardjieff, K. A., Hochtl, P., Segelke, B. W., Tao, F.-M. & Rupp, B. (2002) *Acta Crystallogr. D* **58,** 735–743.
32. Sianidis, G., Karamanou, S., Vrontou, E., Boulias, K., Repanas, K., Kyrpides, N., Politou, A. S. & Economou, A. (2001) *EMBO J.* **20,** 961–970.
33. Baud, C., Karamanou, S., Sianidis, G., Vrontou, E., Politou, A. S. & Economou, A. (2002) *J. Biol. Chem.* **277,** 13724–13731.
34. Kimura, E., Akita, M., Matsuyama, S. & Mizushima, S. (1991) *J. Biol. Chem.* **266,** 6600–6606.
35. Or, E., Navon, A. & Rapoport, T. (2002) *EMBO J.* **21,** 4470–4479.
36. Dempsey, B. R., Economou, A., Dunn, S. D. & Shilton, B. H. (2002) *J. Mol. Biol.* **315,** 831–843.
37. Snyders, S., Ramamurthy, V. & Oliver, D. (1997) *J. Biol. Chem.* **272,** 11302–11306.
38. Karamanou, S., Vrontou, E., Sianidis, G., Baud, C., Roos, T., Kuhn, A., Politou, A. S. & Economou, A. (1999) *Mol. Microbiol.* **34,** 1133–1145.
39. Subramanya, H. S., Bird, L. E., Brannigan, J. A. & Wigley, D. B. (1996) *Nature* **384,** 379–383.
40. Yao, N., Hesson, T., Cable, M., Hong, Z., Kwong, A. D., Le, H. V. & Weber, P. C. (1997) *Nat. Struct. Biol.* **4,** 463–467.
41. Kim, J. L., Morgenstern, K. A., Griffith, J. P., Dwyer, M. D., Thomson, J. A., Murcko, M. A., Lin, C. & Caron, P. R. (1998) *Structure (London)* **6,** 89–100.
42. Velankar, S. S., Soultanas, P., Dillingham, M. S., Subramanya, H. S. & Wigley, D. B. (1999) *Cell* **97,** 75–84.
43. Simon, S. M., Peskin, C. S. & Oster, G. F. (1992) *Proc. Natl. Acad. Sci. USA* **89,** 3770–3774.
44. Kourtz, L. & Oliver, D. (2000) *Mol. Microbiol.* **37,** 1342–1356.